Atmos. Chem. Phys. Discuss., 11, 32245–32282, 2011
www.atmos-chem-phys-discuss.net/11/32245/2011/
doi:10.5194/acpd-11-32245-2011

Atmospheric Chemistry and Physics Discussions

Automated ground-based remote sensing measurements of greenhouse gases at the Białystok site in comparison with collocated in-situ measurements and model data

J. Messerschmidt[1,*], H. Chen[2,], N. M. Deutscher[1], C. Gerbig[2], P. Grupe[1], K. Katrynski[4], F.-T. Koch[2], J. V. Lavrič[2], J. Notholt[1], C. Rödenbeck[2], W. Ruhe[3], T. Warneke[1], and C. Weinzierl[1]**

[1]Institute of Environmental Physics, University of Bremen, Bremen, Germany
[2]Max Planck Institute for Biogeochemistry, Jena, Germany
[3]impres GmbH, Bremen, Germany
[4]AeroMeteoservice, Białystok, Poland

*now at: California Institute of Technology, Pasadena, CA, USA
**now at: NOAA-ESRL, Boulder, CO 80305, USA

Received: 14 September 2011 – Accepted: 21 November 2011 – Published: 8 December 2011

Correspondence to: J. Messerschmidt (janina@caltech.edu)

Published by Copernicus Publications on behalf of the European Geosciences Union.

Abstract

The fully automated observatory for total greenhouse gas (GHG) column measurements introduced here complements the in-situ facilities at the Białystok site in Poland. With the automated Fourier Transform Spectrometer (FTS), solar absorption measurements have been recorded nearly continuously since March 2009. In this article the automation system, including the hardware components and the automation software will be described in its basics. Furthermore the first comparison of the FTS dataset with the collocated in-situ measurements and the first comparison of the Jena CO_2 inversion model are presented. This model identifies monthly variations in the total CO_2 column and the seasonal amplitude is in good agreement with the FTS measurements.

1 Introduction

Until recently remote sensing measurements of greenhouse gases have not been used in atmospheric inversions to determine CO_2 source/sink distributions. Atmospheric inverse transport modeling have traditionally been based on a network of in-situ boundary layer measurement stations. The surface flux distributions were derived from these atmospheric concentration measurements and therewith limited by the sparse spatial coverage of the sampling sites (Marquis and Tans, 2008). Additionally, recent studies showed the sensitivity of the CO_2 sink estimates to the modeled vertical transport. As a result of incorrect vertical transport, a large set of atmospheric inverse model results were inconsistent with total column measurements and vertical aircraft profiles (Baker et al., 2006; Stephens et al., 2007; Yang et al., 2007). By integrating total column measurements within the existing observations, the estimation of the spatial distribution and the temporal variation of the CO_2 sources and sinks is expected to be improved.

Within two EU projects, GEOmon (Global Earth Observation and Monitoring of the Atmosphere) and IMECC (Infrastructure for Measurements of the European Carbon Cycle), the FTS group at the Institute of Environmental Physics (IUP) was responsible

ACPD
11, 32245–32282, 2011

for upgrading the GHG in-situ sites at Białystok (Poland) and Trainou (France) with two automated mobile FTS instruments. These two sites are among the most important sites for GHG in-situ measurements in Europe. Currently these are the only sites in Europe where collocated FTS solar absorption and vertical resolved in-situ measurements, including tall tower and regular aircraft profiling in the boundary layer, are performed. The Białystok site is the easternmost measurement station within Europe. Besides the on-site tall tower (300 m), low aircraft profiling up to 2.8 km is operated regularly.

To measure the background abundances of trace gases, measurement sites are remote from local sources of these gases. The local infrastructure is often rudimentary and an operator only occasionally on-site. Therefore automation of the measurement system is desirable (Washenfelder et al., 2006; Deutscher et al., 2010; Geibel et al., 2010). In order to perform autonomous measurements, maintenance has to be minimized and a maximum of remote control by different remote access possibilities needs to be guaranteed. A sophisticated logging system is aimed at ensuring the system state is recorded at all times, and a basic self-organized error handling allows a minimum of local support.

In the period from August 2007 until August 2009 the FTS automation system was designed and implemented for the two FTS instruments at the IUP in Bremen in collaboration with the company impres GmbH. Different instruments were integrated to one programmable system and the automation strategy and software were developed. The automated FTS system detects the weather conditions, performs measurements along given day specific tasks, executes self-organized error handling and is entirely remote-controlled. During the installation, side-by-side measurements were performed to ensure intercomparability between instruments (Messerschmidt et al., 2010). In February 2009 the first instrument was successfully installed in Białystok, Poland and is operated in close cooperation with AeroMeteoService (Poland). The second instrument was installed at the Trainou site (≈ 20 km northeast of Orléans, France) in August 2009 and is operated in close cooperation with the RAMCES team at LSCE (Gif-sur-Yvette,

ACPD
11, 32245–32282, 2011

France).

This article introduces the automated FTS system exemplified by the Białystok system. The Trainou system is the same, with some adaptation to local conditions (e.g. internet access). Furthermore, the first steps of integrating the total column measurements with the existing observations are done by comparing the Białystok FTS total column measurements with collocated boundary layer in-situ data and a first comparison with the Jena CO_2 inversion model.

2 The automated FTS system

The automation system is constructed for the temperate zone and successfully tested under temperatures from −30 °C to 40 °C. Both the safeness and the stability of the automated system were important criteria in the automation concept. Long lasting and robust components as well as solid constructions and communication interfaces were chosen.

In the following all used hardware components, the automation concept and the automation software are described in their basic function.

2.1 The Hardware

The automation system is housed in a modified 20′ standard shipping container. To minimize the possibility of deformation, parts of the roof were reinforced for the installation of the hutch and the solar tracker. Furthermore the container was insulated for operation in mid-latitudes, supplied with a basic electrical installation and equipped with an air condition to assure internal temperature stability. The voltage supply is protected by an Uninterruptible Power Supply (UPS). All subsystems communicate via an internal network and the system is connected to the internet via multiple paths.

ACPD
11, 32245–32282, 2011

2.1.1 Main PLC

A Programmable Logic Controller (PLC) (the "Main PLC") acts as the central unit responsible for safeguarding the system. In the case of a critical system status, the Main PLC brings the system in a save system state (e.g. hutch cover will be closed during rain or devices will be switched off). Beside this primary task, the Main PLC accumulates the data of the sensor system (weather station and room climate sensors), switches the power supply for central devices in the automation system (air conditioning, hutch system and all parts of the measurement system) and communicates in the daily routine with the Master PC (described in 2.1.2).

2.1.2 Master PC

The Master PC is the host of the automation software and controls the actual measurement tasks. Based on the supplied information of the Main PLC and its own internal analyses, the Master PC controls the measurement system that encompasses the 125HR Bruker FTS instrument (with a lamp cooler and a vacuum pump), the solar tracker and the data storage system.

2.1.3 Hutch system

The main function of the hutch system is to protect the solar tracker from dirt and damage. The hutch system encompasses the hutch cover (Fig. 1), the hutch control cabinet and the compressed air supply (compressor, dryer, condensation drain, pressure vessel). The hutch cover is driven by pneumatic cylinders, which control opening and closing of the hutch. To prevent condensation in the hutch cover on the solar tracker mirrors, a thermal screen and a fan are installed. The fan is switched on if the outside temperature is less than the dew point temperature inside the container.

The main controls of the pneumatic system and the Hutch PLC are mounted in the hutch control cabinet. The Hutch PLC coordinates all actions of the hutch but

ACPD
11, 32245–32282, 2011

is controlled by the Main PLC.

The compressed air supply ensures that the hutch is closed hermetically by pressurizing the seals when no solar measurements should be performed, e.g. during the night or when the weather conditions do not allow the seals to be vented such as during rain or high wind speeds. In the case of a power outage (or failure), the valves are automatically switched in a state that the hutch will be closed. To ensure enough pressure in the pneumatic system in this case, a suitable pressure vessel is installed. As a safety precaution, a manual override is also installed, which when activated causes all seals to be vented and hutch movement to be stopped and enables the hutch cover to be moved by hand.

2.1.4 Solar tracker

The solar tracker was built in the workshop of the University of Bremen. For the positioning of the solar tracker mirrors, the integrated motion controller XPS-C2 together with the rotation stages RV160PP and RV80PP from the company Newport were chosen. This motion controller offers high-speed communication through 10/100 Base-T Ethernet, high trajectory accuracy and wide programming functionality. For manual control a XPS-RC remote control panel was supplied. A detailed description can be found in the documentation available from Newport (www.newport.com).

2.1.5 Fourier Transform Infrared Spectrometer (FTS)

The measurement instrument is a Bruker IFS 125/HR Fourier Transform Infrared Spectrometer. It is optimized to measure gases such as CO_2, CH_4, CO, N_2O, H_2O, HDO, O_2, HF in the near infrared solar region. The maximum resolution is 0.0035 cm^{-1}, and was chosen to allow an upgrade for MIR measurements in the future. A silicon (Si) diode detector, which is sensitive between 11000 cm^{-1}–15 000 cm^{-1} and an Indium-Gallium-Arsenide (InGaAs) diode, which is sensitive within 3800 cm^{-1}–11 000 cm^{-1} are installed. Using a dual channel measurement mode the spectral range from 3800 cm^{-1}

ACPD
11, 32245–32282, 2011

up to 15 000 cm^{-1} can be measured simultaneously within minutes. A Calcium-Fluoride (CaF_2) beam splitter is used. A hydrogen chloride (HCl) cell is permanently mounted in the source compartment of the instrument, allowing the Instrumental Line Shape to be monitored monthly with tungsten lamp measurements (Hase et al., 1999). The measurements are conducted under vacuum to ensure stable, clean and dry conditions within the system. Therefore the system is equipped with an oil-free scroll pump (Varian TriSrcoll300) that evacuates the system over night.

The FTS instrument at Białystok is part of the Total Carbon Column Observing Network (TCCON) (Wunch et al., 2011) and the measurement parameters are adapted for this purpose. Spectra are acquired with 0.014 cm^{-1} resolution, an aperture of 1 mm diameter and a scanner velocity of 10 kHz. The electronic low pass filter is set to 10 kHz (corresponding to 15 798 cm^{-1}). The high folding limit for the Fast Fourier Transformation is set to 15 798 cm^{-1}. Two individual scans, one forward and one backward, are carried out per measurement.

2.1.6 Data storage

During a measurement, the data are stored on a network attached storage (NAS). Each night, the FTS data are copied onto two tapes. Two HP StorageWorks DAT 160 SCSI-tape drives were chosen for this backup. Once a month, one tape is sent to the IUP, while the other tape remains in the container as a data backup. At the IUP, the data are read out with the NovaStore NovaBackup 10.0 software and stored on the data storage system.

2.1.7 Sensor system

To detect the weather conditions and to monitor the room climate the automation system is equipped with several sensors. The weather station consists of sensors for pressure, temperature, humidity, wind speed, rain, and direct solar radiation. The room climate is recorded with temperature sensors and one humidity sensor. The

ACPD
11, 32245–32282, 2011

specifications are found in Table 2.

2.2 Automation concept

The automation system consists of the introduced subsystems: the Main PLC, the Master PC, the hutch system, the measurement system (solar tracker, FTS instrument and data storage system), and the sensor system. Three of these subsystems are the main controlling units: the Main PLC, the Hutch PLC, and the Master PC. Apart from automated activities done by these controlling units, the automation system can be fully controlled by a local or remote operator.

The automation system has two operational states: run mode and sleep mode. A transition between these states as well as a reset of the automation system can be either triggered by the user (direct command input by a local/remote operator) or automatically executed. At this time, the system is in a temporary transition state: initialization mode, going-to-sleep mode, going-to-run mode or reset mode.

A mode for maintenance purposes is additionally provided. In this case, the automation system is switched off and the devices need to be operated manually by an operator inside the container.

2.2.1 Control units

The system can be controlled locally via the Main PLC control cabinet, the hutch control cabinet and the front panel of the automation software on the Master PC. Several LEDs and a LCD display, located at the front panel of the Main PLC control cabinet, indicate the state of the automation system and ongoing actions.

The standard access for the remote control is via Virtual Network Computing (VNC) (for error handling, debugging, remote control of the automation software) and ssh (for uploading updates, filing measurement tasks) to the Master PC. The connection to the Internet from the automated system is minimized for security reasons. Standard tasks using internet connectivity are setting the time, and sending of error/alarm and

ACPD
11, 32245–32282, 2011

warning emails, and data storage status. Additional independent remote access is necessary, e.g. if the Internet connection is affected by an error, therefore a GSM modem (Tixi HG33/HG34) was installed, via which basic functions are executable (run, sleep and reset of the automation system) and basic information (system status, errors) is provided via text messages.

2.3 Automation software

The automation software integrates all instruments and decision-making devices into one automated system. The programming was divided into several subsystems: the PLCs are closed subsystems that were programmed with the software TwinCat, provided by Beckhoff Automation GmbH. The GSM modem was programmed with the software TILA, provided by Tixi.com GmbH. The automation of all other devices was programmed with LabView 8.5 from National Instruments, a dedicated visual programming language for automating measurement systems. The structure of the automation software is modular, and overall 800 submodules were written. The basic modules are pictured in Fig. 2, and their main functions are explained in the following section.

2.3.1 The master program

The Master program is the central unit of the automation software. It parameterizes the automation system, communicates with all devices, especially with the Main PLC and the measurement system, and is responsible for operating the measurements. The Master program initializes measurements, commands the opening of the hutch and the tracking of the sun, requests the setting of FTS parameters and organizes the collection and storage of the measurement data. Additionally, it logs the system state at all times and provides an interface for local and remote operators. The Master program itself works in a loop, which covers the following subroutines

ACPD
11, 32245–32282, 2011

1. checking for local or remote user requests,
2. collecting all necessary information from the modules,
3. analyzing all provided information,
4. executing subsequent actions,
5. commanding tasks to the subsystems, and
6. logging the state of the system.

The main steps of the loop are indicated in Fig. 3. The time of the loop can be set according to the speed at which the modules provide their subsystem states. The main analyzing tool is realized in a simple matrix. The matrix has as columns the states of the subsystems and as rows actions, which follow from a certain system state. If the states of the subsystems (respectively the columns in the matrix) fit a wanted action (respectively a row in the matrix), the action will be communicated by the Master program and executed. If there is no match in the matrix, no action will result out of the analysis. If required this matrix can be easily modified and adapted to specific needs in the system behavior just by editing the matrix in a spreadsheet.

All necessary communication with the subsystems and the action executions takes place in specialized software modules, which will be introduced in the following sections.

2.3.2 The FTS module

The FTS Module controls the communication between the Master program and the FTS instrument. The IFS 125/HR instrument is equipped with an embedded web server (EWS). It is a standard web server/client base. The client, in our case the automation software, only sends requests to the web server and collects data. The EWS has two interfaces, a ftp- and a http-interface. All measurement communication with the

ACPD
11, 32245–32282, 2011

instrument is done via the http-interface. Even in the case when commands have to be send to the EWS, it is done by adding the appropriate query to the requested HTML page. The ftp-interface is used exclusively for firmware updates.

2.3.3 The taskfile module

In order to be able to prescribe tasks in arbitrary time periods, the automation software is equipped with the Taskfile module. Daily tasks can be stored in a simple text file. Thus, the vacuum pump can be switched on and off, measurements can be initialized, e.g. opening of the hutch, moving the solar tracker, different measurement tasks can be filed and data can be written onto tapes.

2.3.4 Further modules

In additional modules the coordination of the solar tracker is realized (Tracker Module) or the theoretical direct solar radiation is calculated and compared to the input from the sensor to detect sunny measurement conditions (Cloud Detection Module). The underlying model for the calculation is a simplified clear sky model for direct and diffuse insolation on horizontal surfaces from Richard E. Bird, Solar Energy Research Institute, Colorado, USA (Bird and Hulstrom, 1981). In a further subroutine the data storage is realized (Data Handling Module). It checks for new files, and prepares the data for storage on tape.

3 TCCON standard data retrieval

The raw data of the interferograms are obtained directly from the embedded web server (EWS) inside the FTS instruments. To calculate the spectra from the interferograms, the SLICE-IPP software developed within the framework of TCCON is used. The software performs the Fast Fourier transformation and corrects the spectra for solar intensity variations, caused e.g. by passing clouds (Keppel-Aleks et al., 2007).

ACPD
11, 32245–32282, 2011

GFIT, a nonlinear least-squares spectral fitting algorithm, developed by G. C. Toon (Jet Propulsion Laboratory, United States), is used for the retrieval of the trace gas column amounts from the measured spectra (Wunch et al., 2010a). In the software an initial vertical profile of gas mole fractions, the a priori profile, is assumed. The tropospheric portion of the a priori CO_2 profile is based on an empirical model fitting GLOBALVIEW CO_2 data (GLOBALVIEW-CO2, 2010). The day and site specific tropopause height is determined from the National Centers for Environmental Prediction/ National Center for Atmospheric Research (NCEP/NCAR) reanalysis. The stratospheric a priori CO_2 decreases with altitude above the tropopause height, depending on the age of the air, based on measurements of Andrews et al. (2001). The site and day specific CO_2 a priori profiles are calculated with meteorological data, e.g. altitude, pressure, temperature and water profiles, taken from NCEP/NCAR re-analysis data interpolated to local noon for the day. The a prior profile is scaled in order to get the best spectral fit to spectra e.g. of the HITRAN database (Rothman et al., 2009). The retrieved profile is integrated and the column-averaged dry-air mole fraction (DMF), e.g. X_{CO_2}, is calculated from the retrieved column amount by

$$X_{CO_2}(p) = \frac{1e6 \cdot \text{column}_{CO_2}}{[\frac{p_s}{m_{air} g} - \text{column}_{H_2O}]} \quad (1)$$

or by

$$X_{CO_2} = \frac{1e6 \cdot \text{column}_{CO_2}}{\frac{\text{column}_{O_2}}{0.2095}} \quad (2)$$

with p_s: surface pressure, m_{air}: mean molecular mass of air and g: density-weighted gravitational acceleration. X_{CO_2} is therefore expressed in $\mu\text{mol}\,\text{mol}^{-1}$, commonly referred to as parts per million [ppm].

Taking the ratio of the atmospheric CO_2 and O_2 columns (Eq. 2) minimizes systematic and correlated errors, e.g. errors in the solar zenith angle, pressure errors,

ACPD
11, 32245–32282, 2011

influence of the instrumental line shape present in both retrieved CO_2 and O_2 columns (Washenfelder et al., 2006; Wunch et al., 2010a).

The CO_2 column is retrieved in two windows centered at 6220 cm^{-1} (window width = 80 cm^{-1}) and 6339.5 cm^{-1} (window width = 85 cm^{-1}). The RMS-error weighted mean is used to calculate X_{CO_2}. Column O_2 is retrieved from the electronic band centered at 7882 cm^{-1} (windows width = 240.00 cm^{-1}). The airmass dependence is corrected with an empirical derived relationship supplied with the software package and described in Wunch et al. (2010a) and Deutscher et al. (2010). Data outside the range [0.20–0.22] for O_2, as well as outside the range [350 ppm–420 ppm] for CO_2 are regarded as outliers in the TCCON standard retrieval and discarded.

All main processing steps are outlined in Fig. 4. Further details on the TCCON retrieval, e.g. sensitivity tests, are found in Wunch et al. (2010a).

All presented measurement data were obtained with SLICE-IPP version 20100123, and the TCCON standard retrieval was performed with GFIT version 4.4.10.

The Białystok FTS instrument was calibrated to WMO standards during the IMECC campaign. The IMECC campaign was the first calibration campaign of six European FTS sites (Messerschmidt et al., 2011). The result of the IMECC campaign, as well as the results of all other calibration campaigns within TCCON, demonstrate that a single global calibration factor can be applied (Deutscher et al., 2010; Wunch et al., 2010b; Washenfelder et al., 2006). The resulting single global calibration factor to WMO scale was applied to the data presented here.

Prior to the 27 September 2009, the Białystok FTS data were systematically affected by a periodic laser mis-sampling, described in Messerschmidt et al. (2010). Following Messerschmidt et al. (2010), these X_{CO_2} data were corrected by +0.96 ppm.

ACPD
11, 32245–32282, 2011

4 FTS measurements in comparison with the collocated tall tower measurements

With a top height of more than 300 m, the Białystok tall tower is one of the tallest in Europe. The gas measurements at the tall tower are operated by the MPI-BGC (Jena, Germany). A variety of atmospheric trace gases have been sampled at five levels (5 m, 30 m, 90 m, 180 m, 300 m) quasi-continuously since 2005. CO_2 volume mixing ratios are measured with a LI-COR LI-7000 NDIR gas analyzer. Further instruments are an Oxzilla FC-2 fuel cell analyzer for O_2 and an Agilent 6890 gas chromatograph for CH_4, CO, N_2O, and SF_6, described in Popa et al. (2010).

Daytime CO_2 time series for three tall tower levels (5 m, 90 m, 300 m) are shown in Fig. 5, and nocturnal CO_2 time series in Fig. 6. All measurements are shown as weekly means of daytime and nocturnal averages for measurements between 12:00 p.m. and 03:00 p.m., and 00:00 a.m. and 05:00 a.m. local time, respectively. The 5 m level is shown in red , the 90 m level in green, and the highest level at 300 m is pictured in blue. Gaps in the data record are due to instrumental failures, e.g. air conditioning problems. The figures show the effects of the covariance between surface fluxes and atmospheric CO_2 transport:

on a diurnal scale, photosynthesis starts after sunrise, leading to CO_2 uptake in the biosphere. Simultaneously the warming leads to a stronger vertical temperature gradient, and the planetary boundary layer (PBL) height rises. With the deeper mixing, lower CO_2 concentrations are transported into the upper troposphere. In contrast, after sunset, the forcing of the vertical temperature gradient stops, and the PBL gets shallower. CO_2 sources due to respiration and decomposition are accumulated near the surface and lead to elevated CO_2 in the lower troposphere. This effect can be seen in Figs. 5 and 6. The daytime CO_2 concentrations are similar at all three levels throughout the year. At all seasons the CO_2 is diluted due to the vertical mixing within the PBL (Fig. 5). In contrast, the nocturnal CO_2 concentrations are different for all tall tower heights, and always the highest near the surface due to the shallow nocturnal

ACPD
11, 32245–32282, 2011

PBL mixing (Fig. 6).

On a seasonal scale, the CO_2 is diluted over land by advection to layers over the ocean. In summer, strong convections lead to a deep PBL mixing, a dilution of the photosynthesis signal and a transport of low CO_2 concentrations to the upper troposphere and advection. In winter, weak convections entail shallow PBL mixing, an accumulation of the respiration signal near the surface and elevated CO_2 concentration in the lower troposphere. This effect explains the stable layering for day times in winter.

Overall, the CO_2 exchange at the surface leads to the largest daytime seasonal cycle at the lowest tall tower level, but is attenuated due to the transport in the upper troposphere.

The FTS time series shows the seasonality of biospheric uptake and respiration, but muted compared to the tall tower measurements. The differences between the FTS data and the tall tower data are smallest in summer, as the photosynthesis signal is diluted through transportation into the upper troposphere. CO_2 concentrations measured at the tall tower are representative of the tropospheric CO_2 concentration and therefore vary in a similar way as the total column measurements. In contrast, the difference is large in winter, as the respiration signal is accumulated at the surface. CO_2 concentrations at the tall tower are elevated compared to the total column measurements.

5 FTS measurements in comparison with the Jena CO_2 inversion model

The Jena CO_2 inversion (JC) estimates surface CO_2 fluxes based on atmospheric CO_2 concentration measurements provided by various institutions (Rödenbeck, 2005). The atmospheric transport is calculated by the global off-line atmospheric transport model TM3 (Heimann and Koerner, 2003). It has a spatial resolution of approximately 4° latitude × 5° longitude × 19 vertical levels and is driven by meteorological fields derived from NCEP data.

A priori information for fossil fuel emissions is derived from the EDGAR v4.0 emission database (Olivier and Berdowski, 2001). The Biome-BGC model is used as land

ACPD
11, 32245–32282, 2011

biosphere net ecosystem exchange (NEE) model, (White et al., 2000; Churkina and Trusilova, 2002). To estimate the ocean CO_2 uptake, an inversion based on ocean carbon data (Gloor et al., 2003; Mikaloff Fletcher et al., 2007) with small scale spatial and seasonal patterns, given by Takahashi et al. (2002), is used. The basic approach is as described in Rödenbeck et al. (2003), with updates described in Rödenbeck (2005) and Rödenbeck et al. (2006). The atmospheric fields and further information are available at: http://www.bgc-jena.mpg.de/~christian.roedenbeck/download-CO2-3D/.

In this work, the special run ana96_v3.3, designed to provide 3-D atmospheric tracer fields, is used. Bialystok data were not used in the flux inversion, which was the basis for the analyzed fields.

5.1 Data analysis

Rodgers and Connor (2003) introduced a method to compare two instruments, of which one has a much higher vertical resolution than the other. This approach is used in the modification described by Wunch et al. (2010b). Only model data for which contemporary FTS measurements exist were considered. FTS measurements can only be taken during sunny weather conditions, therefore the comparison is restricted to these conditions. For each FTS measurement, the nearest model result within one hour was smoothed with the averaging kernel of the FTS measurement. The averaging kernels used for the comparison are shown in Fig. 7, color coded by solar zenith angle. The averaging kernel matrix represents the change in the retrieved X_{CO_2} profile at one level i due to a perturbation to the true X_{CO_2} profile at another level j. Since GFIT performs a profile scaling retrieval (PSR), the averaging kernel matrix reduces to a vector representing the sensitivity of the retrieved total column to perturbations of the partial columns at the various atmospheric levels.

The model profile data have to be integrated to column-averaged CO_2 dry-air mole fractions to be comparable to the FTS measurements. As the JC model does not provide a H_2O profile output, the GFIT a priori H_2O profile, which is based on NCEP data, is used for the integration.

ACPD
11, 32245–32282, 2011

In Fig. 8 the integrated model data are shown compared to the FTS X_{CO_2} time series. In the bottom panel, the FTS daily averages are shown in a black dotted line. The FTS time series exhibits several gaps due to bad weather conditions and instrumental problems, e.g. solar tracker failures, or internal laser breakdown. The associated daily averages of the integrated model data are indicated with a gray dotted line. In the upper panel the difference (FTS minus model data) of the daily averages is shown. The mean of the differences of −1.2 ppm is given as a thin black line. Additionally, the results for the integrated low aircraft measurements, described in Sect. 5.2, are given color coded for each overpass day.

The differences between the FTS data and the model simulation are rather small, but vary periodically with time (Upper panel, Fig. 8). This indicates that to first order, the JC model captures the seasonal amplitude and phase of the column measurements well. This is challenging because it is difficult to model the biospheric uptake in Europe due to the heterogeneously distributed large variety of ecosystems in a rather small land area. The differences are, however, time-dependent and will be further investigated in a multiple year comparison. In a first investigation, the influence of local variations on the integrated model results is analyzed with on-site in-situ data.

5.2 The Jena CO_2 inversion model in comparison with the tall tower measurements

The model outputs at the five level heights of the collocated tall tower are compared with the in-situ data taken at these heights (not all shown). The CO_2 time series for the lowest and the highest level (5 m, 300 m) are pictured in comparison with the model results in Fig. 9. All data are given as weekly averages of daytime measurements between 12:00 p.m. and 03:00 p.m.. The Jena CO_2 inversion captures the seasonal cycle at both levels to the first order, whereas the higher level is better captured, especially in the winter.

The nocturnal time series for both levels are shown in Fig. 10. All data are given as weekly averages of nighttime measurements between 00:00 a.m. and 05:00 a.m.. The

ACPD
11, 32245–32282, 2011

nocturnal seasonal cycle at 300 m is captured, whereas the model fails to modulate the nocturnal CO_2 accumulation at the lowest level (Fig. 10). This could be due to imperfect vertical mixing, e.g. the stable boundary layer during the night is not well represented (Fig. 6), or imperfect fluxes (false partitioning of respiration and gross primary production (GPP) but more or less reasonable net ecosystem exchange (NEE) as constrained by the inversion). If the vertical mixing is wrong, but the fluxes are correct, the 300 m model data would be increased, because the nocturnal accumulated CO_2 would have been transported to higher layers. The good representation of the nocturnal seasonal cycle at 300 m suggests a false partitioning of the NEE.

5.3 The Jena CO_2 inversion model in comparison with low aircraft measurements

The model simulation in the upper PBL and lower free troposhere is investigated with low aircraft profiles taken on a regular base near the Białystok site. The quality of the aircraft data is ensured by comparison to independent CO_2 mixing ratio measurements from an in-situ analyzer, and analyzes of flask samples collected during the flights (Chen et al., 2011). A total of 12 low aircraft profiles were available for the analyzed time period and are listed in Table 1. The measurements were taken in spirals at an average distance of 9 km (between 2 km and 13 km) to the Białystok site.

In order to compare the low aircraft profile measurements, the aircraft profiles and the model profiles are interpolated on the common pressure-grid used for the integration in Sect. 5.1. The low aircraft profiles are compared at pressure levels corresponding to the surface and altitudes of 1, 2, and 3 km to the most contemporary model profile. The time differences between the model profiles and the low aircraft profiles are listed in Table 1. In Fig. 11, the differences between the model and the aircraft profiles are shown color-coded for each of the 12 low aircraft profiles. A CO_2 overestimation by the original model output leads to a positive difference, and vice versa. The thick black line indicates the mean difference for all profiles. The model captures on average the CO_2 at the surface, but the differences have the greatest variability. In altitudes of 1 and

ACPD
11, 32245–32282, 2011

2 km the model overestimates the CO_2, whereas at 3 km the CO_2 is captured again on average.

To compare the total column averages, the aircraft profiles were extended above the aircraft ceiling with the most contemporary model profile. Afterwards, the extended profiles were integrated as described in Sect. 5.1. The differences between the integrated extended low aircraft profiles and the integrated most contemporary model profiles are listed in Table 1. In Fig. 8 the CO_2 total column averages calculated with the extended aircraft profiles are shown color coded for each overpass in comparison to the results calculated with the model profiles. Using the low aircraft measurements leads on average to a downscaling of the associated original model result. Calculated only for the overpass days, it reduces the difference of 0.81 ppm ± 0.49 ppm between the JC model and the FTS data to 0.48 ppm ± 0.79 ppm.

6 Conclusions

The fully automated FTS systems in Białystok was introduced. The underlying automation concept, the hardware and the software were described in their main functions. The minimization of maintenance, the safeness and robustness of the system were key factors in the automation. The automation system offers multiple remote access, as well as the possibility of filing different trace gas measurement tasks for arbitrary time periods. The safeness of the data record is guaranteed by redundant data storage. The ability of the automated system to continuously measure trace gas total columns in the near infrared is demonstrated with the FTS X_{CO_2} dataset presented here.

The first comparison of the Białystok FTS dataset to collocated in-situ boundary layer CO_2 measurements and the Jena CO_2 inversion model was performed. The FTS total CO_2 column measurements show the expected muted seasonal cycle compared to the collocated tall tower CO_2 measurements due to the reduced sensitivity to the local planetary boundary layer. In comparison with the Jena CO_2 inversion model, it is

ACPD
11, 32245–32282, 2011

shown that the model is able to predict monthly variations and the amplitude and the phase of the CO_2 seasonal cycle, despite small time dependent differences. The influence of local variations on the integrated model output was analyzed by using tall tower measurements and low aircraft profiles. The tall tower data indicate a false nocturnal respiration assumed in the JC model and the comparison to the low aircraft profiles points to an overestimation in the upper PBL, which is in agreement with the overestimation seen in the total column measurements. The use of the multiple datasets available at the Białystok site gives additional information about the performance of model simulations and thereby implicates improvements of CO_2 sink estimations.

Acknowledgements. The Bialystok FTS instrument was automated with funding from the Senate of Bremen and the EU projects IMECC (Infrastructure for Measurement of the European Carbon Cycle) and GEOmon (Global Earth Observation and Monitoring). The maintenance and logistical work is kindly provided by AeroMeteo Service (Bialystok) and RAMCES team at LSCE (Gif-sur-Yvette, France). We acknowledge financial support by NASA's Program, grant number NNX11AG016, Constraining fluxes of carbon with total column measurements of CO_2 and CH_4.

References

Andrews, A. E., Boering, K. A., Daube, B. C., Wofsy, S. C., Loewenstein, M., Jost, H., Podolske, J. R., Webster, C. R., Herman, R. L., Scott, D. C., Flesch, G. J., Moyer, E. J., Elkins, J. W., Dutton, G. S., Hurst, D. F., Moore, F. L., Ray, E. A., Romashkin, P. A., and Strahan, S. E.: Mean ages of stratospheric air derived from in situ observations of CO_2, CH_4, and N_2O, J. Geophys. Res., 106, 32295–32314, 2001. 32257

Baker, D. F., Law, R. M., Gurney, K. R., Rayner, P., Peylin, P., Denning, A. S., Bousquet, P., Bruhwiler, L., Chen, Y.-H., Ciais, P., Fung, I. Y., Heimann, M., John, J., Maki, T., Maksyutov, S., Masarie, K., Prather, M., Pak, B., Taguchi, S., and Zhu, Z.: TransCom 3 inversion intercomparison: Impact of transport model errors on the interannual variability of regional CO_2 fluxes, 1988-2003, Global Biogeochem. Cycles, 20, GB1002, doi:10.1029/2004GB002439, 2006. 32247

ACPD

11, 32245–32282, 2011

Bird, R. E. and Hulstrom, R. L.: Simplified Clear Sky Model for Direct and Diffuse Insolation on Horizontal Surfaces, Technical Report SERI/TR-642-761, Solar Energy Research Institute, 1981. 32256

Chen, H., Winderlich, J., Gerbig, C., Katrynski, K., Jordan, A., and Heimann, M.: Validation of routine continuous airborne CO_2 observations near the Bialystok Tall Tower, Atmos. Chem. Phys., accepted, 2011. 32263

Churkina, G. and Trusilova, K.: A global version of the biome-bgc terrestrial ecosystem model, Tech. rep., Max Planck Institute for Biogeochemistry, Jena, 2002. 32261

Deutscher, N. M., Griffith, D. W. T., Bryant, G. W., Wennberg, P. O., Toon, G. C., Washenfelder, R. A., Keppel-Aleks, G., Wunch, D., Yavin, Y., Allen, N. T., Blavier, J.-F., Jiménez, R., Daube, B. C., Bright, A. V., Matross, D. M., Wofsy, S. C., and Park, S.: Total column CO_2 measurements at Darwin, Australia -Ű site description and calibration against in situ aircraft profiles, Atmos. Meas. Tech., 3, 947–958, doi:10.5194/amt-3-947-2010, 2010. 32248, 32258

Geibel, M. C., Gerbig, C., and Feist, D. G.: A new fully automated FTIR system for total column measurements of greenhouse gases, Atmos. Meas. Tech., 3, 1363–1375, doi:10.5194/amt-3-1363-2010, 2010. 32248

GLOBALVIEW-CO2: Cooperative Atmospheric Data Integration Project – Carbon Dioxide,NOAA-ESRL, Boulder, Colorado, cD-ROM, 2010. 32257

Gloor, M., Gruber, N., Sarmiento, J., Sabine, C. L., Feely, R. A., and Rödenbeck, C.: A first estimate of present and preindustrial air-sea CO_2 flux patterns based on ocean interior carbon measurements and models, Geophys. Res. Lett., 30, 10-1–10-4, 2003. 32261

Hase, F., Blumenstock, T., and Paton-Walsh, C.: Analysis of the Instrumental Line Shape of High-Resolution Fourier Transform IR Spectrometers with Gas Cell Measurements and New Retrieval Software, Appl. Optics, 38, 3417–3422, 1999. 32252

Heimann, M. and Koerner, S.: The global atmospheric tracer model TM3, Technical Report 5, Max-Planck-Institut für Biogeochemie, 2003. 32260

Keppel-Aleks, G., Toon, G. C., Wennberg, P. O., and Deutscher, N. M.: Reducing the impact of source brightness fluctuations on spectra obtained by Fourier-transform spectrometry, Appl. Optics, 46, 4774–4779, 2007. 32256

Marquis, M. and Tans, P.: Carbon Crucible, Science, 320, 460–461, 2008. 32247

Messerschmidt, J., Macatangay, R., Notholt, J., Petri, C., Warneke, T., and Weinzierl, C.: Side by side measurements of CO_2 by ground-based Fourier transform spectrometry (*FTS*), Tellus B, 62, 749–758, doi:10.1111/j.1600-0889.2010.00491.x, 2010. 32248, 32258

ACPD
11, 32245–32282, 2011

Messerschmidt, J., Geibel, M. C., Blumenstock, T., Chen, H., Deutscher, N. M., Engel, A., Feist, D. G., Gerbig, C., Gisi, M., Hase, F., Katrynski, K., Kolle, O., Lavric, J. V., Notholt, J., Palm, M., Ramonet, M., Rettinger, M., Schmidt, M., Sussmann, R., Toon, G. C., Truong, F., Warneke, T., Wennberg, P. O., Wunch, D., and Xueref-Remy, I.: Calibration of TCCON column-averaged CO_2: the first aircraft campaign over European TCCON sites, Atmos. Chem. Phys., 11, 10765–10777, doi:10.5194/acp-11-10765-2011, 2011. 32258

Mikaloff Fletcher, S. E., Gruber, N., Jacobson, A. R., Gloor, M., Doney, S. C., Dutkiewicz, S., Gerber, M., Follows, M., Joos, F., Lindsay, K., Menemenlis, D., Mouchet, A., Müller, S. A., and Sarmiento, J. L.: Inverse estimates of the oceanic sources and sinks of natural CO_2 and the implied oceanic carbon transport, Global Biogeochem. Cycles, 21, GB1010, doi:10.1029/2006GB002751, http://dx.doi.org/10.1029/2006GB002751, 2007. 32261

Olivier, J. G. J. and Berdowski, J. J. M.: The Climate System, chap. Global emissions sources and sinks, pp. 33–78, Publishers/Swets & Zeitlinger Publishers, Lisse, The Netherlands, ISBN: 90-5809-255-0, 2001. 32260

Popa, M. E., Gloor, M., Manning, A. C., Jordan, A., Schultz, U., Haensel, F., Seifert, T., and Heimann, M.: Measurements of greenhouse gases and related tracers at Bialystok tall tower station in Poland, Atmospheric Measurement Techniques, 3, 407–427, doi:10.5194/amt-3-407-2010, 2010. 32259

Rödenbeck, C.: Estimating CO_2 sources and sinks from atmospheric mixing ratio measurements using a global inversion of atmospheric transport, Technical report 6, Max Planck Institute for Biogeochemistry, Jena, 2005. 32260, 32261

Rödenbeck, C., Houweling, S., Gloor, M., and Heimann, M.: CO_2 flux history 1982-Ű2001 inferred from atmospheric data using a global inversion of atmospheric transport, Atmos. Chem. Phys., 3, 1919–1964, doi:10.5194/acp-3-1919-2003, 2003. 32261

Rödenbeck, C., Conway, T. J., and Langenfelds, R.: The effect of systematic measurement errors on atmospheric CO_2 inversions: a quantitative assessment, Atmos. Chem. Phys. Discuss., 5, 8979–9001, doi:10.5194/acpd-5-8979-2005, 2005. 32261

Rodgers, C. D. and Connor, B. J.: Intercomparison of remote sounding instruments, J. Geophys. Res., 108, 13-1–13-14, 2003. 32261

Rothman, L., Gordon, I., Barbe, A., Benner, D., Bernath, P., Birk, M., Boudon, V., Brown, L., Campargue, A., Champion, J.-P., Chance, K., Coudert, L., Dana, V., Devi, V., Fally, S., Flaud, J.-M., Gamache, R., Goldman, A., Jacquemart, D., Kleiner, I., Lacome, N., Lafferty, W., Mandin, J.-Y., Massie, S., Mikhailenko, S., Miller, C., Moazzen-Ahmadi, N., Naumenko, O.,

ACPD
11, 32245–32282, 2011

Nikitin, A., Orphal, J., Perevalov, V., Perrin, A., Predoi-Cross, A., Rinsland, C., Rotger, M., Simecková, M., Smith, M., Sung, K., Tashkun, S., Tennyson, J., Toth, R., Vandaele, A., and Auwera, J. V.: The HITRAN 2008 molecular spectroscopic database, J. Quant. Spectrosc. Ra., 110, 533–572, doi:10.1016/j.jqsrt.2009.02.013, hITRAN, 2009. 32257, 32275

Stephens, B. B., Gurney, K. R., Tans, P. P., Sweeney, C., Peters, W., Bruhwiler, L., Ciais, Philippe AN DRamonet, M., Bousquet, P., Nakazawa, T., Aoki, S., Machida, T., Inoue, G., Vinnichenko, N., Lloyd, J., Jordan, A., Heimann, M., Shibistova, O., Langenfelds, Ray L., Steele, L. P., Francey, R. J., and Denning, A. S.: Weak Northern and Strong Tropical Land Carbon Uptake from Vertical Profiles of Atmospheric CO_2, Science, 316, 1732–1735, doi:10.1126/science.1137004, 2007. 32247

Takahashi, T., Sutherland, S., Sweeney, C., Poisson, A., Metzl, N., Tilbrook, B., Bates, N., Wanninkhof, R., Feely, R., Sabine, C., and Olafsson, J., and Nojiri, Y.: Global sea-air CO_2 flux based on climatological surface ocean pCO_2, and seasonal biological and temperature effects Global sea-air CO_2 flux based on climatological surface ocean pCO_2, and seasonal biological and temperature effects, Deep-Sea Res. Pt. II, 49, 1601–1622, 2002. 32261

Washenfelder, R., Toon, G., Blavier, J.-F., Yang, Z., Allen, N., Wennberg, P., Vay, S., Matross, D., and Daube, B.: Carbon dioxide column abundances at the Wisconsin Tall Tower site, J. Geophys. Res., 111, 1–11, doi:10.1029/2006JD007154, 2006. 32248, 32258

White, M. A., Thornton, P. E., Running, S. W., and Nemani, R. R.: Parameterization and Sensitivity Analysis of the BIOME-BGC Terrestrial Ecosystem Model: Net Primary Production Controls, Earth Interact., 4, 1–85, 2000. 32261

Wunch, D., Toon, G. C., Blavier, J.-F. L., Washenfelder, R., Notholt, J., Connor, B. J., Griffith, D. W. T., Sherlock, V., and Wennberg, P. O.: The Total Carbon Column Observing Network Debra Wunch, Geoffrey C. Toon, Jean-François L. Blavier, Rebecca A. Washenfelder, Justus Notholt, Brian J. Connor, David W. T. Griffith, Vanessa Sherlock and Paul O. Wennberg, Phil. Trans. R. Soc. A 2011 369, 2087–2112, doi:10.1098/rsta.2010.0240, 2010a. 32257, 32258

Wunch, D., Toon, G. C., Wennberg, P. O., Wofsy, S. C., Stephens, B. B., Fischer, M. L., Uchino, O., Abshire, J. B., Bernath, P., Biraud, S. C., Blavier, J.-F. L., Boone, C., Bowman, K. P., Browell, E. V., Campos, T., Connor, B. J., Daube, B. C., Deutscher, N. M., Diao, M., Elkins, J. W., Gerbig, C., Gottlieb, E., Griffith, D. W. T., Hurst, D. F., Jiménez, R., Keppel-Aleks, G., Kort, E. A., Macatangay, R., Machida, T., Matsueda, H., Moore, F., Morino, I., Park, S., Robinson, J., Roehl, C. M., Sawa, Y., Sherlock, V., Sweeney, C., Tanaka, T., and Zondlo, M. A.: Calibration of the Total Carbon Column Observing Network using aircraft profile data,

ACPD
11, 32245–32282, 2011

Atmos. Meas. Tech., 3, 1351–1362, doi:10.5194/amt-3-1351-2010, 2010b. 32258, 32261
Wunch, D., Toon, G. C., Blavier, J.-F. L., Washenfelder, R. A., Notholt, J., Connor, B. J., Griffith, D. W. T., Sherlock, V., and Wennberg, P. O.: The Total Carbon Column Observing Network, Philos. T. R. Soc. A, 369, 2087–2112, doi:10.1098/rsta.2010.0240, http://rsta.royalsocietypublishing.org/content/369/1943/2087.abstract, 2011. 32252
Yang, Z., Washenfelder, R., Keppel-Aleks, G., Krakauer, N., Randerson, J., Tans, P., Sweeney, C., and Wennberg, P.: New constraints on Northern Hemisphere growing season net flux, Geophys. Res. Lett., 34, L12807, doi:10.1029/2007GL029742, 2007. 32247

ACPD
11, 32245–32282, 2011

Table A1. Low aircraft overpasses available for the analyzed time period at the Białystok site. The date, the time difference to nearest available model output, the distance and altitude range are listed. The last column shows the difference between the integrated extended low aircraft profiles and the integrated most contemporary model result.

date [dd-mmm HH:MM-HH:MM]	Δt (JC-in-situ) [HH:MM]	dist. range [km]	alt. range [km]	Δ (JC- assembled JC) [ppm]
31 Mar, 14:09–15:21	02:09	2.44–13.32	0.09–2.47	0.00
8 Apr, 08:48–10:06	02:48	1.74–12.28	0.09–2.52	−0.44
27 Apr, 15:35–16:53	03:35	2.58–13.49	0.09–2.53	0.25
15 May, 14:45–15:51	08:45	1.24–13.07	0.08–2.47	0.41
29 May, 10:29–11:30	−00:30	1.21–52.50	0.12–2.54	0.13
15 Jun, 11:44–12:56	00:00	0.92–14.04	0.09–2.62	0.68
29 Jun, 11:08–12:09	00:00	2.24–13.08	0.11–2.67	0.43
7 Jul, 10:29–11:42	−00:15	2.54–13.15	0.07–2.63	−0.05
18 Jul, 08:51–10:04	01:56	2.55–13.38	0.11–2.65	2.21
10 Aug, 13:10–14:18	−16:49	2.15–17.59	0.11–2.79	1.09
25 Aug, 11:30–11:38	−00:22	3.04–13.83	0.10–0.34	−0.42
27 Nov, 11:13–11:49	−00:11	2.64–13.00	0.10–1.47	−0.36

ACPD
11, 32245–32282, 2011

Table A2. The weather station specifications. In order to detect reliable measurement conditions, sensors are installed for: pressure, temperature, humidity, wind speed, rain, direct solar radiation. To monitor the room climate stability, four temperature sensors are distributed within the container.

sensor	model	range	precision	remarks
pressure	PTB220 Vaisala	500 hPa.. 1100 hPa	0.1 hPa	calibrated with reference sensor at least once a year
temperature	Hygro-Thermogeber Compact 1.1005.54.241 Thies Clima	−30 °C.. +70 °C	±0.3 °C	protected by Wetter- und Strahlungsschutz compact
humidity		0 %..100 %	±2 %	
wind speed	Windgeber-Compact 4.3519.05.141 Thies Clima	$0.5\frac{m}{s}..50\frac{m}{s}$	$\pm0.5\frac{m}{s}$ (±3 % of measurand)	internal heater
rain	Niederschlags-waechter 5.4103.10.000 Thies Clima	yes/no	rain detection conditions are manually adjustable	optical sensor
sun	CSD3 Kipp&Zonen	0..1V	$1mV/\frac{W}{m^2}$ ±33 % at $120\frac{W}{m^2}$	direct solar radiation
		yes/no		sun duration (threshold $120\frac{W}{m^2}$)
	to prevent condensation and snow/ice cover: 1. heat level (1 W, 12 V) controlled by the Thies junction box 2. heat level (10 W, 12 V) switched by the Main PLC ($T < 5$ °C)			
room temperature and humidity	4 × PT100 distributed within the container (1 × rack, 2 × FTS, 1 × roof penetration)			

ACPD
11, 32245–32282, 2011

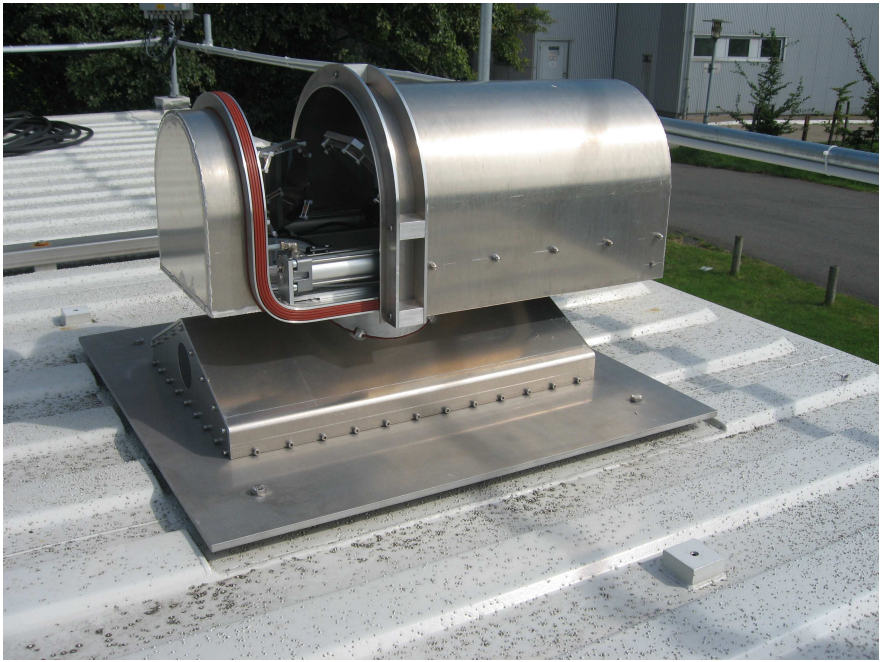

Fig. 1. The mounted hutch cover in its opened position. The red seals can be pressurized to close the hutch hermetically. The solar tracker mirrors and the pneumatic cylinder that controls the movement of the hutch cover are located inside the hutch.

ACPD
11, 32245–32282, 2011

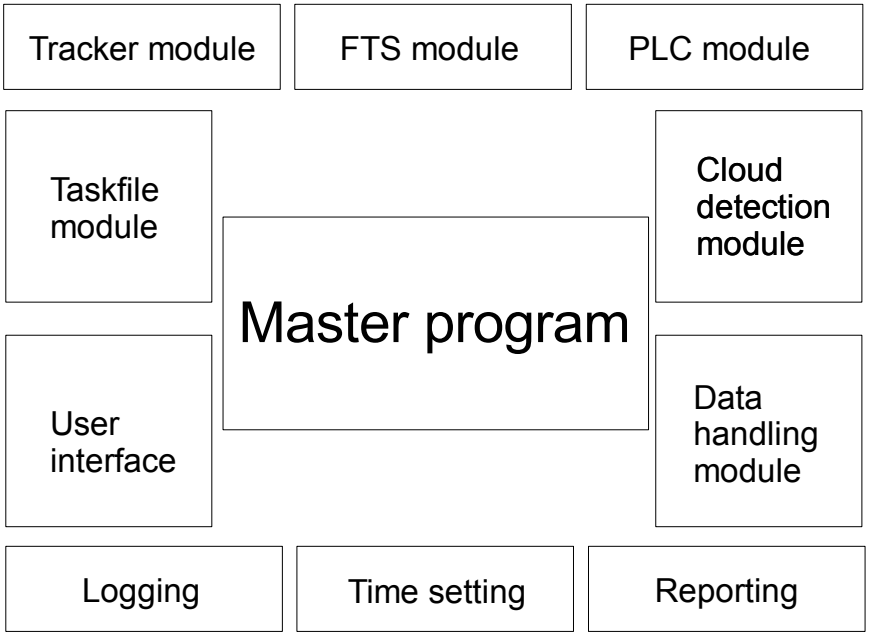

Fig. 2. Schematic of the interacting modules within the automation software. The fact that the Master Program is central to the function of the software is evident. At the top the major modules for the measurement process are shown. On the right, supplemental modules for the measurement process are grouped. On the left, the provided modules for the local and remote access are indicated. At the bottom, logging tools and the time setting are summarized.

ACPD
11, 32245–32282, 2011

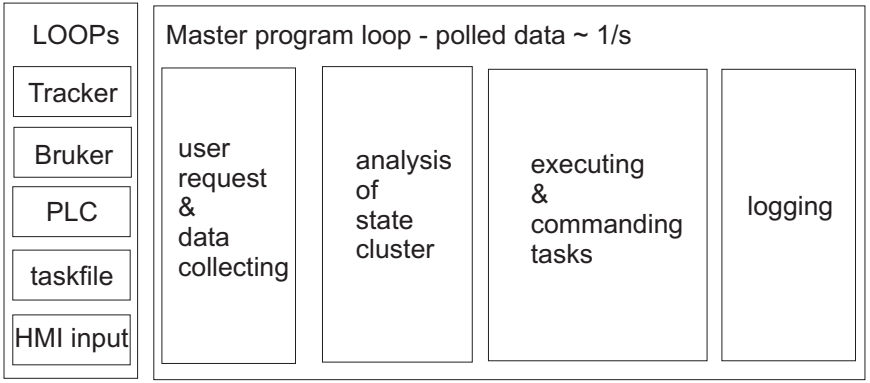

Fig. 3. The basic dynamical structure of the automation program. All submodules provide the update of their parameters in a loop process. The Master program itself is set up in a loop process. It checks for local or remote user requests, collects the provided information of the submodules and analyzes these information. By commanding tasks to the subsystems, it executes subsequent actions. At the end of one loop, it logs all information as the state of the automation system.

ACPD
11, 32245–32282, 2011

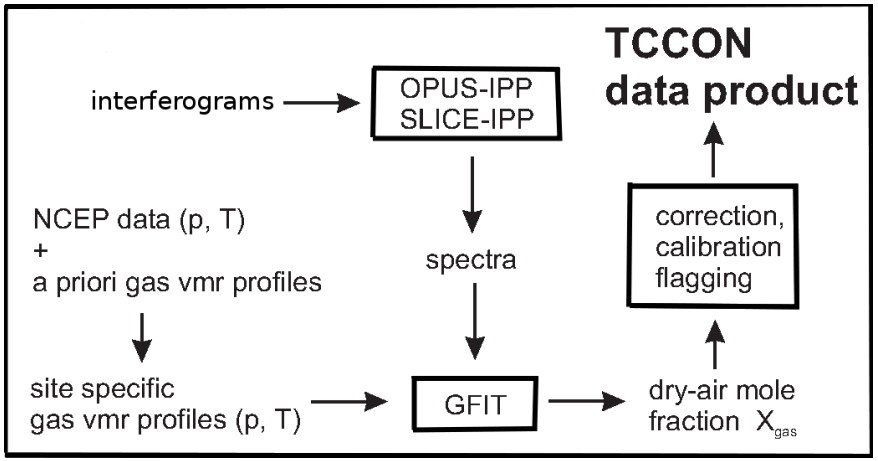

Fig. 4. The software used for the retrieval of atmospheric column-averaged dry-air mole fractions. The main processes are outlined: The measured interferograms are transformed into spectra with the OPUS-IPP or SLICE-IPP software. The a priori profile is approximated with NCEP/NCAR analysis data for the measurement site and day. In GFIT the initial vertical gas mole fraction profile, the a priori profile, is scaled to fit best spectra e.g. of the HITRAN database (Rothman et al., 2009). After correction, calibration and data flagging, the TCCON product are column-averaged dry-air mole fractions X_{gas}.

ACPD
11, 32245–32282, 2011

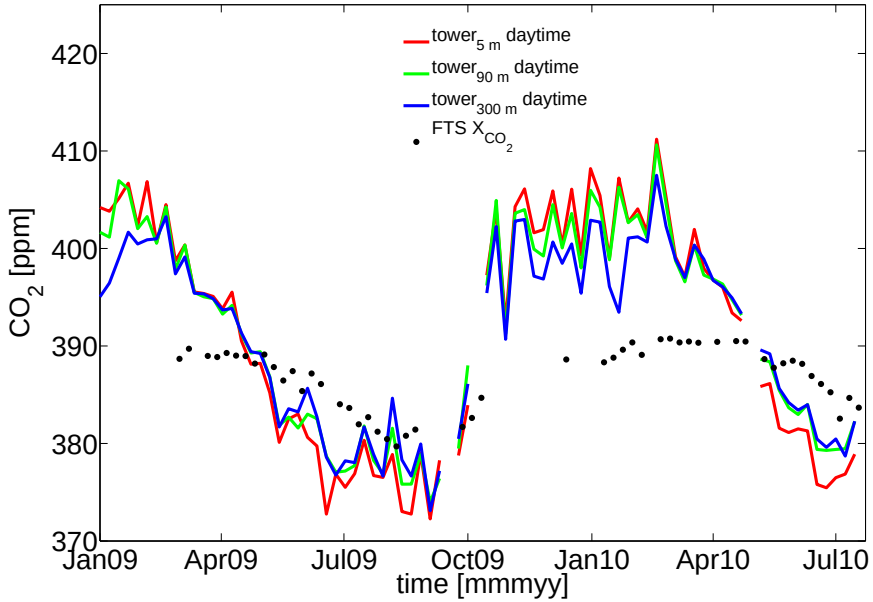

Fig. 5. The daytime CO_2 time series for three tall tower levels (5 m, 90 m, 300 m) highlighting the seasonal cycle in comparison with the FTS measurements. All measurements are shown as weekly averages of daytime measurements between 12:00 p.m. and 03:00 p.m. local time. Gaps in the in-situ data record are due to instrumental problems.

ACPD
11, 32245–32282, 2011

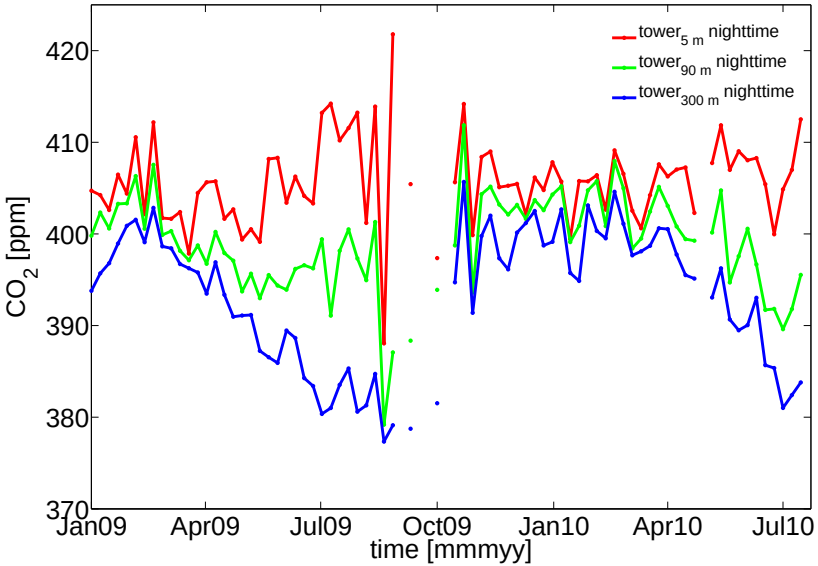

Fig. 6. The nocturnal CO_2 time series for three tall tower levels (5 m, 90 m, 300 m) highlighting the seasonal cycle. The measurements are shown as weekly averages of nighttime measurements between 00:00 am and 05:00 am local time. Gaps in the in-situ data record are due to instrumental problems.

ACPD
11, 32245–32282, 2011

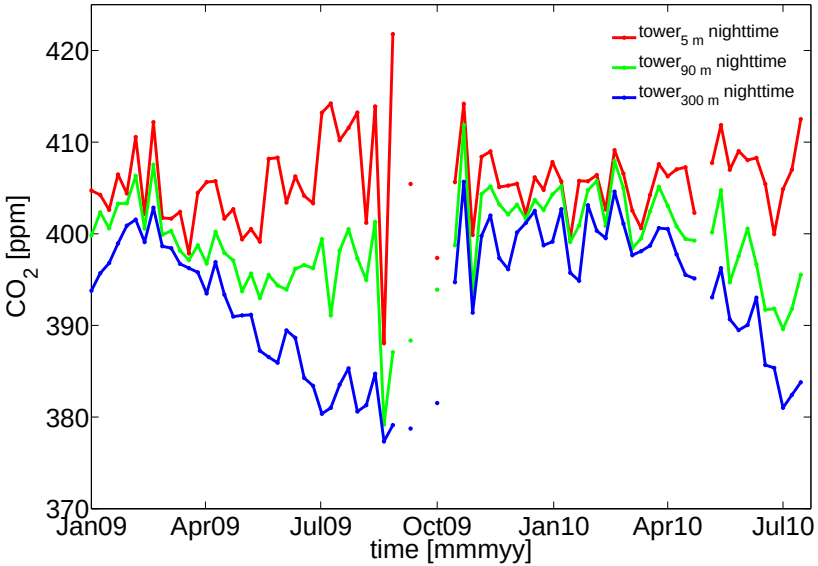

Fig. 7. CO_2 averaging kernels for the presented Białystok FTS measurements color coded for different solar zenith angles. The averaging kernels have no distinct maximum and are constant to first approximation within the troposphere and vary primarily due to different solar zenith angles.

ACPD
11, 32245–32282, 2011

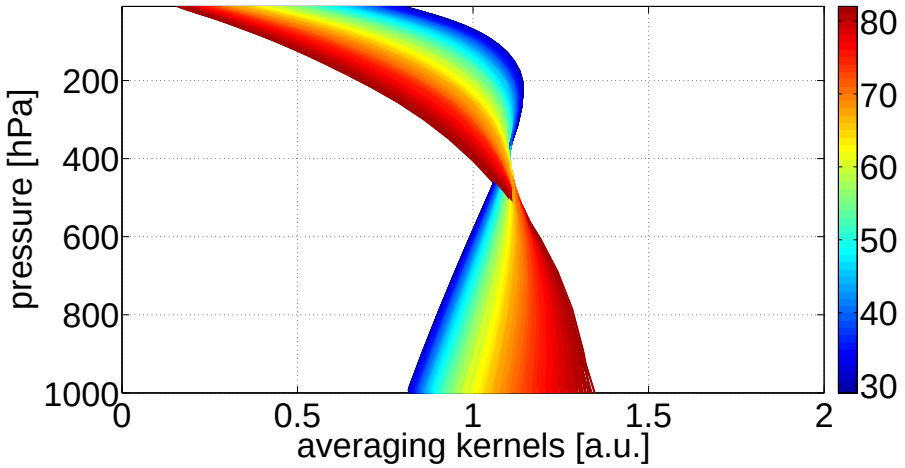

Fig. 8. Upper panel: The difference between the Białystok FTS daily averages and the corresponding integrated model data. The black line indicates the mean difference. The integrated low aircraft measurements, extended above the aircraft ceiling by the model are given color coded for the different overpasses (Sect. 5.2). Bottom panel: the integrated model data of the Jena CO_2 inversion (JC) in comparison with the FTS time series.

ACPD
11, 32245–32282, 2011

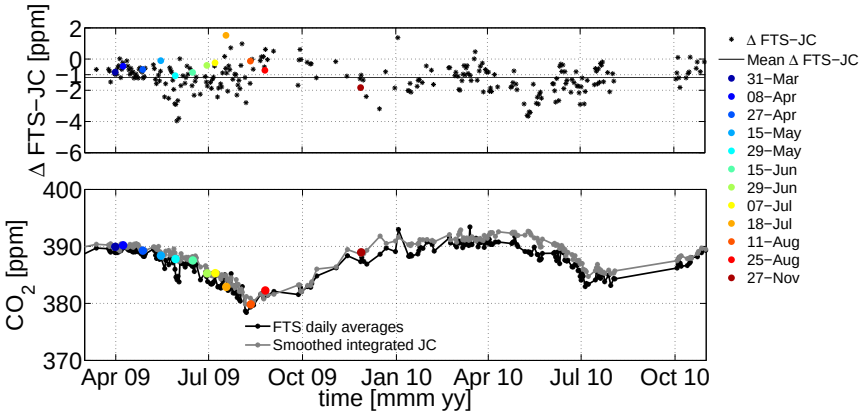

Fig. 9. The JC model output at the lowest and highest level of the tall tower (5 m, 300 m). Weekly averages of daytime measurements between 12:00 p.m. and 03:00 p.m. are compared. The Jena CO_2 inversion captures the seasonal cycle at both levels to the first order, whereas especially in the winter the higher level is better captured.

ACPD
11, 32245–32282, 2011

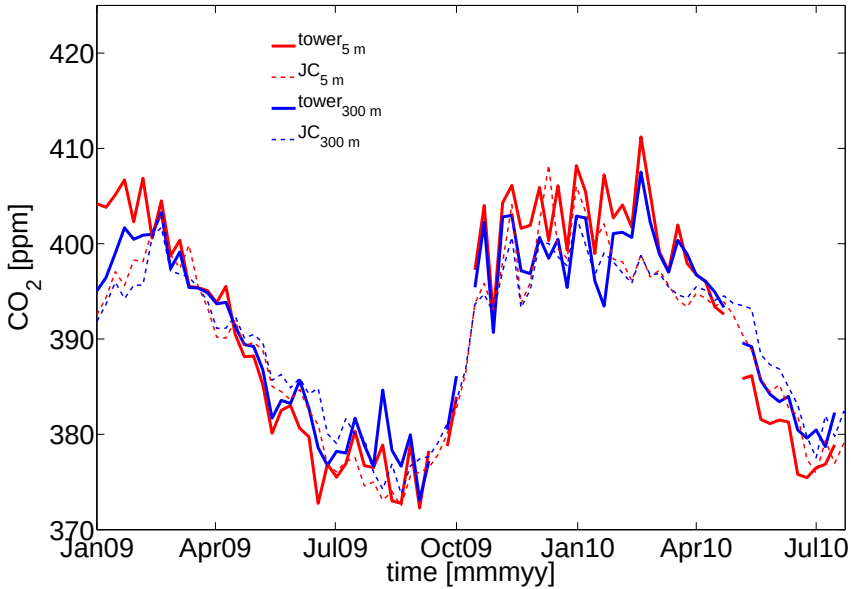

Fig. 10. The JC model output at the lowest and highest level of the tall tower (5 m, 300 m). Weekly averages of nighttime measurements between 00:00 a.m. and 05:00 a.m. are compared. The model captures the seasonal cycle at the upper level, but fails to simulate the nighttime CO_2 accumulation at the ground.

ACPD
11, 32245–32282, 2011

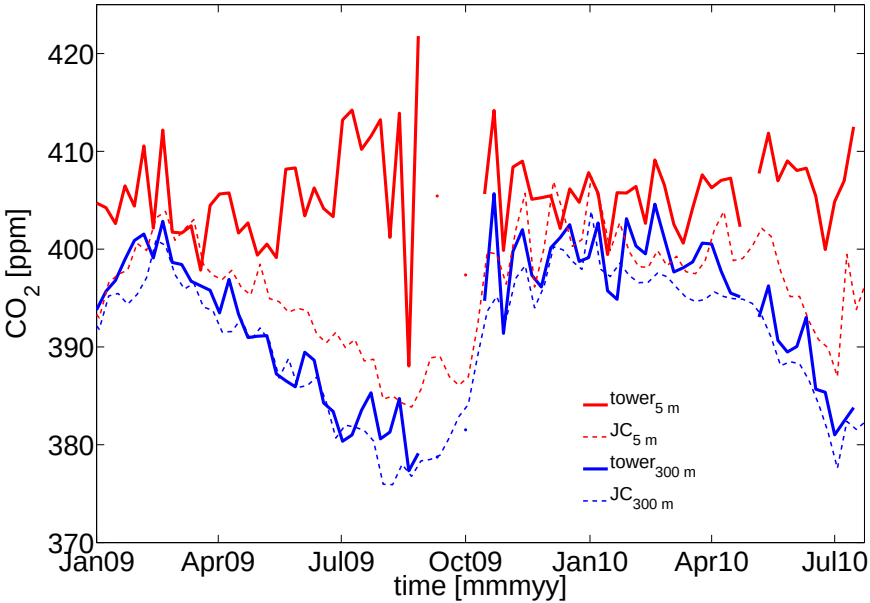

Fig. 11. Difference between the model profiles and contemporary low aircraft profiles on the common pressure-grid used for the integration in Sect. 5.1. For the analyzed time period overall 12 low aircraft profiles up to 2.8 km were conducted, shown color-coded for each overpass. The mean of the differences is given with a black line. At the ground and in 3 km, the JC model captures the CO_2 on average and significantly overestimates it in 1 and 2 km.

ACPD
11, 32245–32282, 2011